High-resolution laser spectroscopy of NO2 just above the (X)over-tilde(2)A(1)-(A)over-tilde(2)B(2) conical intersection

Biesheuvel, C. A.; Bulthuis, J.; Janssen, M. H. M.; Stolte, S.; Snijders, J. G.

Published in:
Journal of Chemical Physics

DOI:
10.1063/1.477640

High-resolution laser spectroscopy of NO_2 just above the $\tilde{X}\,^2A_1$-$\tilde{A}\,^2B_2$ conical intersection: Transitions of $K_-=0$ stacks

C. A. Biesheuvel, J. Bulthuis, M. H. M. Janssen, S. Stolte, and J. G. Snijders

Citation: J. Chem. Phys. **109**, 9701 (1998); doi: 10.1063/1.477640
View online: https://doi.org/10.1063/1.477640
View Table of Contents: http://aip.scitation.org/toc/jcp/109/22
Published by the American Institute of Physics

High-resolution laser spectroscopy of NO_2 just above the $\tilde{X}\,^2A_1-\tilde{A}\,^2B_2$ conical intersection: Transitions of $K_-=0$ stacks

C. A. Biesheuvel,[a] J. Bulthuis, M. H. M. Janssen, and S. Stolte
Department of Physical and Theoretical Chemistry, Vrije Universiteit, de Boelelaan 1083, 1081 HV Amsterdam, The Netherlands

J. G. Snijders
Department of Chemical Physics and Materials Science Centre, Rijksuniversiteit Groningen, Nijenborgh 4, 9747 AG Groningen, The Netherlands

(Received 15 July 1998; accepted 2 September 1998)

The visible absorption spectrum of NO_2 is very dense and irregular, and shows signs of a chaotic frequency and intensity distribution in the higher energy region. The complexity of the spectrum is related to a conical intersection of the potential energy surfaces of the two lowest electronic states. Above the conical intersection strong vibronic interactions lead to hybrid eigenstates, which can be viewed as mixtures of low vibrational levels of the electronically excited state and high vibrational levels of the electronic ground state. As a contribution to the elucidation of the nature of the vibronic bands of NO_2 we have measured high-resolution spectra of a number of vibronic bands in the region between 10 000 and 14 000 cm^{-1} by exciting a supersonically cooled beam of NO_2 molecules with a narrow-band Ti:Sapphire ring laser. The energy absorbed by the molecules was detected by a bolometer, and in some cases, laser-induced fluorescence was detected. The hyperfine structure is dominated by the Fermi-contact interaction and the magnitude of this interaction is a direct measure of the (electronic) composition of the hybrid eigenstates. In the present paper we have restricted our analysis to transitions of $K_-=0$ stacks. The fine- and hyperfine structure of each rotational transition can be analyzed by using an effective Hamiltonian approach. The very good agreement that is found between the calculated transition strengths and the measured line intensities is evidence that in the spectral region studied, rovibronic interactions play a minor role. The composition of the hybrid eigenstates is compared with *ab initio* calculations reported in the literature, leading to the conclusion that measurements of the hyperfine structure are a helpful tool in characterizing vibronic bands. © *1998 American Institute of Physics.* [S0021-9606(98)01446-9]

I. INTRODUCTION

The dominant factor determining the exceedingly complex visible absorption spectrum of NO_2 is the conical intersection of the $\tilde{X}\,^2A_1$ and $\tilde{A}\,^2B_2$ electronic states, proposed by Gillispie *et al.*[1] in 1975. Numerous spectroscopic studies have been made since. The most comprehensive recent studies have been carried out by the group of Jost, Delon and Georges in Grenoble.[2–7] High-resolution absorption spectroscopy of vibronic bands in the $\tilde{A}\,^2B_2$ state was carried out by Demtröder *et al.*[8–11] and very recently by Romanini *et al.*[12] More recent theoretical studies that have contributed much to the understanding of the NO_2 spectrum are those by Hirsch, Buenker, and Petrongolo *et al.*[13–17]

Theoretically,[18] the intersection of the potential energy curves of the first electronically excited state of $^2B_2$ symmetry and the electronic ground state of $^2A_1$ symmetry is found to occur at an O–N–O bond angle of 107.4° at an energy of about 10 000 cm^{-1} above the minimum of the ground state potential.[15] In the adiabatic representation, crossing of the potential energy curves for $Q_3\neq 0$, the antisymmetric stretch coordinate, is not allowed. In the neighborhood of the resulting conical intersection, the adiabatic electronic wave functions vary strongly with the nuclear coordinates. In the diabatic representation this problem is obviated, and the potential energy surfaces are allowed to cross, but here the potential energy is nondiagonal and, in case of NO_2, the diabatic states are strongly coupled by the antisymmetric stretch mode of b_2 symmetry. In general, the resulting hybrid eigenstates will be composed of several vibrational levels in the first diabatic electronically excited state and several vibrational levels in the diabatic electronic ground state. Specifically, above the conical intersection the vibronic B_2 levels can be built of a_1 vibrational levels in the $^2B_2$ electronic state as well as the high b_2 vibrational levels in the $^2A_1$ electronic ground state that are coupled to the former states. Owing to this coupling, the otherwise dark transitions to the highly excited vibrational levels of the electronic ground state borrow intensity from low-lying vibrational levels of the electronically excited state. This explains the dense spectra with many more lines than expected on the basis of only the first electronically excited state.

By measuring high-resolution spectra of vibronic bands, resolving hyperfine splittings, in the region just above the conical intersection, we hope to contribute to the understanding of the nature of those vibronic bands. The main contribution to the hyperfine interaction is the Fermi-contact inter-

[a]Present address: Chemistry Department, University of Rochester, Rochester, NY.

action. The Fermi-contact interaction will vanish in a spin-restricted one-determinant description of a pure $^2B_2$ excited state.[19] In the electronic ground state the Fermi-contact constant is 147.26 MHz.[20] Therefore, the magnitude of the hyperfine constant of the hybrid excited state is a direct measure of the contribution of the two diabatic electronic states in the hybrid excited state.

In a preliminary account of this high-resolution study, we reported on measurements of the vibronic band at 13 352.67 cm^{-1} and an analysis of the hyperfine structure of parts of the $K_- = 0$ and $K_- = 1$ stacks.[21] In the present paper we present results of bolometric measurements of high-resolution spectra of 16 vibronic bands of NO_2 in the energy range of 11 210–13 680 cm^{-1}. Two vibronic bands (13 510.96 cm^{-1} and 13 395.65 cm^{-1}) were, in addition, measured by laser induced fluorescence (LIF). We also tried to measure the vibronic band at 13 477.11 cm^{-1} by LIF, but the intensity appeared to be too weak as to be detectable in our setup.

The total number of $^2B_2$ vibronic states, $b_2\,\tilde{X}\,^2A_1$ and $a_1\,\tilde{A}\,^2B_2$, in the energy range of 11 200–16 150 cm^{-1} was calculated by Georges *et al.*[4] and found to be 271. For the energy range investigated in the present study, roughly 11 000–13 500 cm^{-1}, the averaged density of vibronic bands of $^2B_2$ symmetry is about 1 per 25 cm^{-1}.[4] Measuring the vibronic bands with resolution of the hyperfine structure was only feasible on the basis of previous measurements of those bands by Georges *et al.*, using their ICLAS method.[4] We will refer to the assignments by these authors by labeling the vibronic bands with the band origins as given in their paper. Apart from the band origin, they also determined the absolute value of the fine structure constant, and the $\overline{B'}$ rotational constants for the different rotational levels of the excited state. We will, in addition, determine two hyperfine constants as well as the sign of the fine structure constant. This enables us to locate all hyperfine levels for a given rotational level, and to determine the contribution of both diabatic electronic states in the excited hybrid state.

The measured absorption spectra are simplified by reduction of the number of lines as a consequence of cooling the rotational degrees of freedom in a supersonic jet,[22] favoring population of the lowest rotational levels. In this paper we therefore restrict ourselves to the analysis of the transitions of the $K_- = 0$ stack only and we will defer the discussion of results for transitions of the $K_- = 1$ stack to a following paper.

In Sec. II the experimental setup and conditions are described. In Sec. III the theory underlying vibronic interactions and fine- and hyperfine structure of rotational transitions for the specific case of NO_2 is briefly outlined, in order to present the framework for the spectral analysis (Sec. III B). The results of the bolometric and fluorescence measurements are presented and discussed in Sec. IV. Emphasis will be on the electronic decomposition of the excited hybrid eigenstates and on the correlation between band intensity and contribution of electronic ground state character to the excited state. A summary of the most important results and conclusions is given in Sec. V.

II. EXPERIMENT

The experiments are performed in a molecular beam machine consisting of a source chamber, an interaction chamber and a bolometer chamber. Dependent on the type of experiments, fluorescence measurements or bolometric measurements (see Fig. 1), the interaction chamber needs some small adjustments.

A 5% NO_2/He molecular beam with a backing pressure of 0.5 bar is used. About 5 mm downstream of the quartz nozzle (internal diameter 90 μm) the molecular jet is collimated by a conical skimmer with an aperture of 0.656 mm. The skimmer is attached to the flange connecting the source chamber and the interaction chamber and can be translated over 1 cm from outside the vacuum. The rotational temperature for NO_2 is determined to be about 8 K, using LIF.

The heart of the machine is the interaction chamber, where the laser beam crosses the molecular beam. The interaction chamber is slightly different for the two detection methods. The fluorescence setup will be described first.

A. Fluorescence detection

The laser beam crosses the molecular beam perpendicularly, 25 cm downstream of the nozzle. To reduce background light, predominantly from scattered laser light, light baffles are used to guide the laser into the molecular beam machine.

The molecular beam is modulated with a mechanical (50% on, 50% off) chopper at 120 Hz. The fluorescence light is focused on a photomultiplier tube (RCA 31034), placed on top of the interaction chamber by a homemade telescope system, of which the focus is externally adjustable. The photomultiplier is cooled to $-20\,^\circ$C and used at a voltage of -1500 V. The fluorescence light was filtered with one RG780 filter, reducing the background current to 3×10^{-11} A at a laser power of about 400 mW at 13 510 cm^{-1}. The fluorescence signal is detected by a phase-sensitive detector with a Q-factor of 100 and an RC-time of 1 s. The data points are stored in a personal computer every 1.5 s. The setup allows laser induced fluorescence spectra to be measured with a Doppler linewidth of about 30 MHz.

A drawback of photomultipliers is their low sensitivity in the infrared (RCA C31034: typical spectral response range 200–900 nm). In the case of fluorescence of NO_2 in the infrared there are additional problems. For the $\tilde{A}\,^2B_2 \leftarrow \tilde{X}\,^2A_1$ transitions the Franck–Condon factors for excitations in the infrared are small. So, the absolute fluorescence yield is low, and in addition it is less efficiently measured. Moreover, when the excited hybrid state has mainly an electronic ground state character, the fluorescence yield will be low anyway.

B. Bolometric detection

For the bolometer experiments a multipass cell is installed in the interaction chamber, and the light baffles are replaced by windows. The optimum in keeping a nicely collimated laser beam, without overlap of the laser spots on the multipass mirrors, was found to be at 29 passes. Then the laser comes in at an angle of about 2° with the normal to the

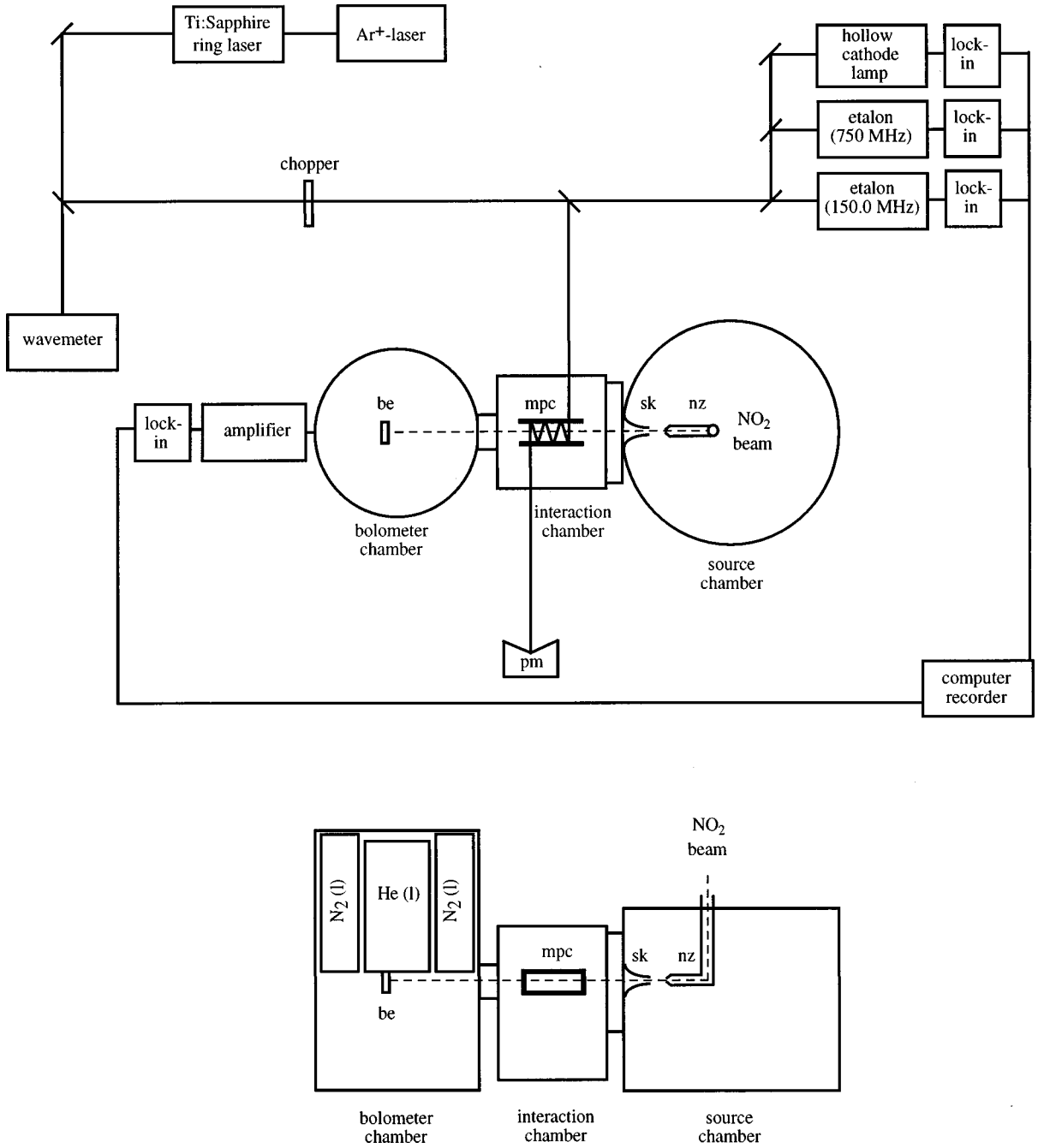

FIG. 1. Schematic experimental setup for the optothermal experiments (top and side view); be=bolometer element; mpc=multipass cell; sk=skimmer; nz=nozzle; pm=power meter.

molecular beam (and the multipass cell). This results in a Doppler shift of about 45 MHz to the blue.[23,24] The laser beam is modulated with a mechanical 50% open–50% closed chopper at 80–120 Hz. After leaving the interaction zone with the laser beam, the molecular beam is skimmed by a 1.5 cm diameter aperture which is just in front of the valve separating the interaction chamber from the bolometer.

The bolometer chamber holds the bolometer device, consisting of a 3.0 l helium dewar, a 6.2 l nitrogen dewar and a composite silicon bolometer element. The element is located at 57 cm from the nozzle and cooled to a temperature of 1.6 K. The molecular beam is skimmed by two apertures in the liquid nitrogen and liquid helium shields, leading to a residual Doppler linewidth of the absorption spectra of about 7 MHz. This reduction of the Doppler width in the bolometer spectra is due to the much smaller cone of accceptance of the molecular beam compared with the LIF spectra.

The bolometer output is preamplified by a factor of 1000 and is further amplified and demodulated by a phase-sensitive detector with a Q-factor of 100 and an RC-time of 300 ms. Per second 3 data points, spaced about 1 MHz, are stored in a personal computer.

The noise-equivalent-power of the detector is measured to be 1.2×10^{-13} W/$\sqrt{\text{Hz}}$ at 1.6 K, at an applied bias voltage of 9 V and a root mean square noise of $V_{\text{noise}}^{\text{rms}}=90$ nV, with a

full load of the molecular beam. After typically 3–4 hours the bolometer starts becoming noisier due to the increased spiking from, mainly, evaporation of NO_2 from the bolometer element.

C. Laser system

The laser, used to record the high-resolution absorption spectra, is a single frequency Ti:Sapphire ring laser, which is actively stabilized.[25,26] The advantages of a Ti:Sapphire laser over infrared dye lasers and diode lasers are its high output power, large tuning range, and high stability. The high power, combined with the narrow linewidth over a broad tuning range, make this type of laser very suitable to do high-resolution spectroscopy.

The Ti:Sapphire ring laser is pumped by all-lines from a large frame Spectra-Physics beam-locked argon ion laser. The output power is about 750 mW at 765 nm with a 6 W pump. The laser has a bandwidth of about 500 kHz and is continuously tunable over the energy range of 750–1050 nm. The spectra are recorded with a scanspeed of 3 MHz/s.

For the absolute determination of the wavelength a Burleigh WA-4500 wavemeter, with an accuracy of 600 MHz is used, which is sufficient to locate the different lines in a vibronic band. For the calibration of the wavelength in the infrared, the optogalvanic signals from an uranium hollow cathode lamp (Cathodeon Limited) and the emission wave numbers from the atlas of Palmer[27] are occasionally used.

Even more important is a stable relative wavelength calibration, which is done with a home-made temperature stabilized interferometer ($\pm 0.2\,^{\circ}\mathrm{C}$). This interferometer is a confocal etalon of 50 cm length, with a free spectral range of 150.0 ± 0.2 MHz. Owing to a finesse over 30 we can assign positions relative to each other with an accuracy of better than 1 MHz. The temperature drift is less than 5 MHz/hour. To concatenate adjacent scans a 750 MHz confocal etalon is used.

III. THEORY AND ANALYSIS

A. Theory

The fine strucure splitting of the rotational levels is due to the coupling between the spin of the unpaired electron and the molecular rotation. There are two contributions to this spin-rotation coupling, a direct one, which is small for NO_2,[28,29] and an indirect one. The direct coupling is mediated by the magnetic field induced by the molecular rotation. If the vibronic level splittings are large compared to the rotational splittings, the indirect coupling can be written as a second order perturbation term, involving the electron spin–electron orbital angular momentum coupling on the one hand, and the Coriolis interaction between the electronic and vibrational angular momentum and the total (orbital) angular momentum on the other hand. This implies that the indirect contribution to the spin-rotation can be expressed as an effective Hamiltonian that is diagonal in the vibronic states.

Following Lin,[29] we write the spin-rotation Hamiltonian as

$$H_{\mathrm{SI}} = \sum_{i,j} \epsilon_{ij} N_i S_j . \tag{1}$$

For NO_2, which has C_{2v} symmetry, only the diagonal elements ϵ_{ii} are nonzero. The coefficients ϵ_{ii} have two contributions, one from the (small) direct coupling and the other from the indirect spin-rotation coupling. The expectation value of the spin-rotation interaction is given by

$$E_{\mathrm{SR}}(N,K) = c(J,N,S)\,\epsilon_{NK} N(N+1), \tag{2}$$

where

$$c(J,N,S) = \frac{J(J+1) - N(N+1) - S(S+1)}{2N(N+1)}, \tag{3}$$

and

$$\epsilon_{NK} = \tfrac{1}{2}(\epsilon_{bb} + \epsilon_{cc}) + [N(N+1)]^{-1}[\epsilon_{aa} - \tfrac{1}{2}(\epsilon_{bb} + \epsilon_{cc})] \times K_-^2 \pm \tfrac{1}{4}\delta_{|K_-|\,1}(\epsilon_{bb} - \epsilon_{cc}). \tag{4}$$

The molecular axes are labeled in the conventional way by a, b, and c in the order of increasing inertial moment about the corresponding axis.

For $K_- = 0$, which is the case we consider here, only the first term at the right hand side of Eq. (4) survives, which we will denote as $\bar{\epsilon}$,

$$\bar{\epsilon} = \epsilon_{NK}(K_- = 0) = (\epsilon_{bb} + \epsilon_{cc})/2. \tag{5}$$

The effective Hamiltonian model mentioned above breaks down if the rovibronic interactions become too large.[30] This breakdown is characterized by a quadratic dependence of the second order energy correction on the rotational quantum number N.

The hyperfine contribution is mainly due to the Fermi-contact term, which is proportional to the electron spin density at the nitrogen nucleus.[29] After averaging over all spatial coordinates, the Fermi-contact interaction is described by the effective Hamiltonian

$$H_{\mathrm{Fermi}} = \sigma \mathbf{I}\cdot\mathbf{S}, \tag{6}$$

$$\sigma = \frac{16\pi}{3} g_{\mathrm{I}} \mu_{\mathrm{B}} \mu_{\mathrm{I}} [\rho_\alpha^s(0) - \rho_\beta^s(0)], \tag{7}$$

in which g_{I} is the nuclear Landé factor, μ_{B} and μ_{I} are the Bohr and nuclear magneton, respectively, and $\rho_\alpha^s(0)$ and $\rho_\beta^s(0)$ are the α and β electron spin density at the nitrogen nucleus, respectively. In a spin-restricted one-determinant description σ reduces to

$$\sigma = \frac{16\pi}{3} g_{\mathrm{I}} \mu_{\mathrm{B}} \mu_{\mathrm{I}} |\Psi(0)|^2, \tag{8}$$

in which $|\Psi(0)|^2$ is the density of the odd electron at the nitrogen nucleus.

The other contribution to the hyperfine term is due to the dipolar spin–spin interaction,

$$H_{\mathrm{SI}} = -g_{\mathrm{S}} g_{\mathrm{I}} \mu_{\mathrm{B}} \mu_{\mathrm{I}} r^{-3} [\mathbf{I}\cdot\mathbf{S} - 3r^{-2}(\mathbf{I}\cdot\mathbf{r})(\mathbf{S}\cdot\mathbf{r})], \tag{9}$$

where g_{S} is the g-factor of the electron spin and $\mathbf{r}$ connects both spins.

Since for a molecule belonging to the C_{2v} point-group only two spin-spin parameters are nonzero,[31] this interaction, after averaging over the electronic and vibrational coordinates, can be written as the effective Hamiltonian[29]

$$H_{\mathrm{SI}}=\lambda(\mathbf{I}\cdot\mathbf{S}-3I_aS_a)+\tau[(I_b+iI_c)(S_b+iS_c)+(I_b-iI_c)(S_b-iS_c)], \tag{10}$$

where

$$\lambda=-g_{\mathrm{S}}g_{\mathrm{I}}\mu_{\mathrm{B}}\mu_{\mathrm{I}}\langle ve|\frac{3r_a^2-r^2}{2r^5}|ve\rangle, \tag{11}$$

$$\tau=\frac{3}{4}g_{\mathrm{S}}g_{\mathrm{I}}\mu_{\mathrm{B}}\mu_{\mathrm{I}}\langle ve|\frac{r_b^2-r_c^2}{r^5}|ve\rangle. \tag{12}$$

The components of $\mathbf{r}$ along the inertial axes are indicated by r_a, r_b, and r_c. The last dipole-dipole interaction constant in Eq. (12), τ, vanishes for $K_-=0$.[29]

Alternatively, the expressions given above for the fine- and hyperfine structure can be written in terms of spherical tensors, see Refs. 28, 32; in those references also useful relationships are given between various notations.

In the diabatic basis the excited vibronic state, $|\Psi_n\rangle$, is, in general, a linear combination of several vibrational levels, $|\chi_{jB}\rangle$, in the first diabatic electronically excited state, $|\phi_B\rangle$, and several vibrational levels, $|\chi_{iA}\rangle$, in the diabatic electronic ground state, $|\phi_A\rangle$

$$|\Psi_n\rangle=\sum_i c_{iA}^n|\chi_{iA}\rangle|\phi_A\rangle+\sum_j c_{jB}^n|\chi_{jB}\rangle|\phi_B\rangle, \tag{13}$$

$$=|\chi_A^n\rangle|\phi_A\rangle+|\chi_B^n\rangle|\phi_B\rangle, \tag{14}$$

in which the $|\chi_A^n\rangle$ and $|\chi_B^n\rangle$ in Eq. (14) are linear combinations of vibrational wave functions in the corresponding diabatic electronic state.[8-10, 33]

The Fermi-contact term of the excited state, $|\Psi_n\rangle$, in the one-determinantal approximation can be written as[33]

$$(H_{\mathrm{Fermi}})_n=\langle\hat{\sigma}\rangle_n\mathbf{I}\cdot\mathbf{S}, \tag{15}$$

$$\langle\hat{\sigma}\rangle_n=(\langle\chi_{b_2}^n|\langle\phi_{A_1}|+\langle\chi_{a_1}^n|\langle\phi_{B_2}|)\hat{\sigma}(|\chi_{b_2}^n\rangle|\phi_{A_1}\rangle+|\chi_{a_1}^n\rangle|\phi_{B_2}\rangle), \tag{16}$$

$$=\langle\chi_{b_2,A_1}^n|\chi_{b_2,A_1}^n\rangle\langle\phi_{A_1}|\hat{\sigma}|\phi_{A_1}\rangle+\langle\chi_{a_1,B_2}^n|\chi_{a_1,B_2}^n\rangle\times\langle\phi_{B_2}|\hat{\sigma}|\phi_{B_2}\rangle, \tag{17}$$

$$=q_{A_1}^n\langle\phi_{A_1}|\hat{\sigma}|\phi_{A_1}\rangle+q_{B_2}^n\langle\phi_{B_2}|\hat{\sigma}|\phi_{B_2}\rangle, \tag{18}$$

$$=q_{A_1}^n\sigma_{A_1}+q_{B_2}^n\sigma_{B_2}, \tag{19}$$

where $\hat{\sigma}$ is the operator corresponding to the average value in Eq. (7); the coefficients $q_{A_1}^n$ and $q_{B_2}^n$ are the contributions of the two diabatic electronic states to the hybrid vibronic state ($q_{A_1}^n+q_{B_2}^n=1$); σ_{A_1} and σ_{B_2} are the Fermi-contact interaction constants of the electronic ground state and first electronically excited state, respectively.

In the spin-restricted one-determinant approximation, the Fermi-contact interaction constant is zero in the first electronically excited state, so the value of the Fermi-contact interaction constant is a direct measure of the weight of the electronic ground state in the hybrid eigenstate

$$\langle\hat{\sigma}\rangle_n=q_{A_1}^n\sigma_{A_1}. \tag{20}$$

Generally, the fine structure splitting is significantly larger than the hyperfine structure splitting. Therefore, the most obvious starting point in coupling the angular momenta will be the *J*-coupling scheme (see Fig. 2).

This means that first the electron spin, $\mathbf{S}(S=1/2)$, is coupled with the rotational angular momentum, $\mathbf{N}$, to an intermediate angular momentum, $\mathbf{J}$ ($\mathbf{J}=\mathbf{N}+\mathbf{S}$), which is then coupled with the nitrogen spin, $\mathbf{I}(I=1)$, to the total angular momentum $\mathbf{F}$. In general the strongest lines are transitions with $\Delta N=\Delta J=\Delta F$.

If the fine structure splitting is smaller than the splitting caused by the spin–spin interaction, the *J*-coupling scheme should be replaced by the *G*-coupling scheme ($\mathbf{G}=\mathbf{I}+\mathbf{S}$, $\mathbf{F}=\mathbf{N}+\mathbf{G}$).

Of course, the final results are independent of the coupling scheme used, provided the complete Hamiltonian is diagonalized in either basis.

B. Analysis

The (hyper)fine structure for the $K_-=0$ stack can be determined using three adjustable parameters, the fine structure constant $\overline{\epsilon'}=(\epsilon'_{bb}+\epsilon'_{cc})/2$ [Eq. (2)], the Fermi-contact interaction constant σ' [Eq. (7)] and the dipole–dipole interaction constant λ' [Eq. (10)].

The experimental spectrum consists of data points with a mutual spacing of about 1 MHz. The lines in the experimental spectra are deconvoluted by assuming a Gaussian line shape. Relative line positions are determined by interpolation from the fringes of the 150.0 MHz temperature stabilized etalon. In this manner the relative frequencies of the transitions are determined with an accuracy of a few MHz. The strongest transition in the experimental spectrum is used as a reference for the calculated frequencies as well as for the calculated relative intensities.

The nonlinear least-squares procedure of Levenberg–Marquardt[34] is used to fit the fine structure constant and the hyperfine structure constants of the excited state to the relative transition frequencies, each with an estimated error. The relative intensities of the transitions are not included in the fit procedure. On the other hand, the agreement between the relative intensities in the calculated and experimental spectra is evidence of the absence of substantial rovibronic interactions.

The *J*-coupling scheme was used as a basis for the calculation of the energy levels and transition frequencies. Convenient expressions for the matrix elements of fine- and hyperfine couplings are given by Lin[29] in the *J*- as well as the *G*-coupling scheme. As stated before, the results are indepen-

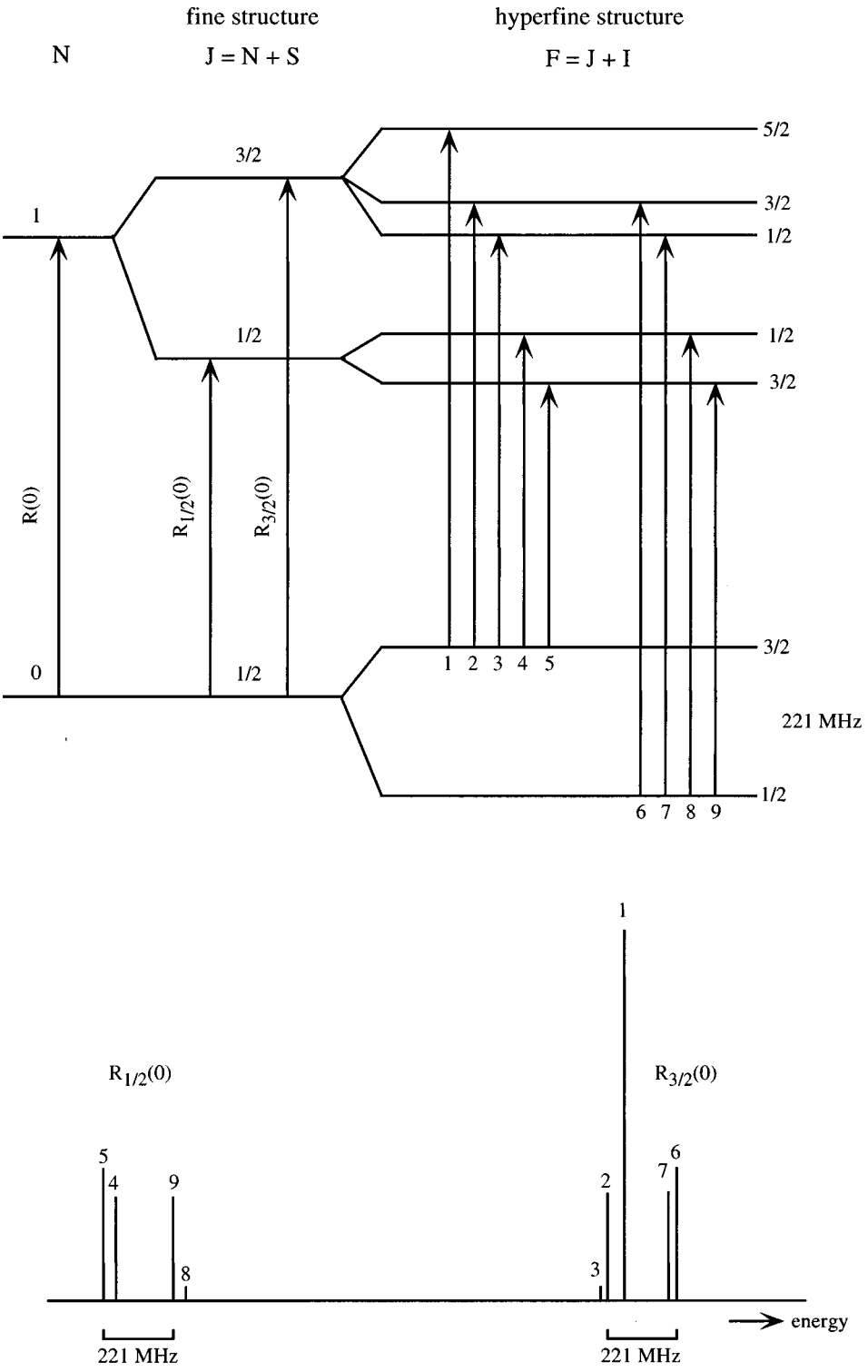

FIG. 2. Positions of the hyperfine structure levels of the $R(0)$ subband of the vibronic band at 13 510.96 cm^{-1}. Note that the energy level spacings between ground and excited state are not drawn to scale. The stick spectrum (bottom) is the theoretical spectrum in the *J*-coupling limit.

dent of the choice of basis, but the assignment of the lines is made somewhat easier by using the *J*-coupling scheme, since this is the scheme that is approximately encountered in the majority of the experimental spectra.

For some vibronic bands we have measured the $R(0)$ and $R(2)$ transitions, which excite different rotational levels, namely $N'=1$ and $N'=3$, respectively. This enables us to determine an average rotational constant $B'=(B'+C')/2$ for the vibronic bands of interest.

The contribution of the electronic ground state and the first electronically excited state to the excited hybrid state will be estimated by resolving the fitted Fermi-contact inter-

action constant into the Fermi-contact interaction constants of both diabatic electronic states involved [Eq. (19)].

In the spin-restricted one-determinant description, the Fermi-contact interaction vanishes for the pure first electronically excited $^2B_2$ state.[19] Van Lenthe[35] calculated the Fermi-contact constant, using density functional theory, for the first electronically excited diabatic state in equilibrium, including spin polarization.[36] He found a negative value of about -10 MHz, which was only weakly dependent on the chosen equilibrium geometry and bond lengths, and always much smaller than the Fermi-contact constant for the electronic ground state. Including spin polarization effects, the calculated Fermi-contact constant for the equilibrium geometry of the electronic ground state ($\theta_e \approx 134°$) is 142 MHz,[37] slightly smaller than the experimental value of 147.263 111 MHz.[20] Increasing the bond angle to 150° decreases the calculated Fermi-contact constant only with about 8 MHz.[37]

For the electronic ground state we use the fine- and hyperfine structure constants determined by Bowman and De Lucia:[20] $\epsilon''_{aa}=5406.539$ MHz, $\epsilon''_{bb}=7.707$ MHz and $\epsilon''_{cc}=-95.266$ MHz, $\sigma''=147.263\,111$ MHz and $\lambda''=11.070$ MHz and $\tau''=14.406$ MHz. The ϵ''_{aa} and τ'' values are given for completeness; they do not enter the transition frequencies for the $K_-=0$ stacks considered here.

For several vibronic bands the transitions to different rotational levels of the $K_-=0$ stack are measured. For those vibronic bands an averaged rotational constant B' is determined by calculating the positions of the associated rotational levels N'' and N' (without fine- and hyperfine structure) and using the formula for the rotational energy in the prolate top limit

$$E_{NK_-}=\overline{B}N(N+1)+(A-B)K_-^2. \tag{21}$$

In determining an averaged rotational constant $\overline{B'}$ for the excited state, an averaged rotational constant $\overline{B''}=0.422$ cm^{-1} is used for the electronic ground state.[20]

IV. RESULTS AND DISCUSSIONS

A. Bolometric measurements

The results from the measured transitions of the $K_-=0$ stack of the vibronic bands in the energy range 11 210–13 680 cm^{-1}, are given in Tables I and II.

Table I lists the band origin and the intensity of the band as measured by Georges *et al.* by their ICLAS method,[4] the frequency of the measured subband and the fit parameters $\overline{\epsilon'}$, σ' and λ' of the excited state. The reported standard deviations correspond to a confidence interval of 95%. Occasionally, an averaged rotational constant $\overline{B'}$ of the excited state is given.

In Table II the decomposition of the excited hybrid state into the two diabatic electronic states is given. The fourth column of Table II gives the contribution of the electronic ground state to the hybrid excited state in the spin-restricted one-determinant approximation, which means that the Fermi-contact interaction term for the first electronically excited state is zero. The fifth column of Table II gives the contribution of the electronic ground state to the hybrid state taking spin polarization into account as explained above. Clearly, the effect of spin polarization is small.

Of more than half of the measured vibronic bands we have measured the $P(2)$ $K_-=0$ subband in addition to the $R(0)$ $K_-=0$ subband. This gives an independent check of the parameters obtained. Both transitions excite the same $N'=1$ final rotational level and the fitting of the experimental data should result in the same parameters describing the excited hybrid state.

As an example we consider the $R(0)$ and $P(2)$ subbands of the vibronic band at 12 724.06 cm^{-1} as shown in Figs. 3(a) and 3(b), respectively. At the experimental rotational temperature of about 8 K the $N''=0$ and $N''=2$ rotational levels are almost equally populated. So the $R(0)$ and $P(2)$ subbands are expected to be of similar intensity. The constants fitted for the excited rotational level obtained from the $R(0)$ and $P(2)$ subbands are in good agreement (see Table I). Figure 3(a) and especially Fig. 3(b) show the excellent agreement between the calculated spectra and the experimental spectra. The experimental intensities are reproduced very well in the calculated spectra.

For vibronic bands where all transitions of the $P(2)$ subband can be assigned, the errors of the fit parameters are expected to be slightly smaller than for the fit parameters obtained from the $R(0)$ subband, because there are more lines in the former case. Nevertheless, we normally measure the $R(0)$ subband for its clear spectrum and thus relatively easy assignment of the transitions. The similarity of the parameters obtained from independent fits of the $R(0)$ subband and the $P(2)$ subband is a check on the correctness of the assignment and the precision of the parameters.

There is one exception to the excellent agreement between calculated and experimental intensities. For the vibronic band at 12 658.34 cm^{-1} a mismatch is found between the fine structure components of the $R(0)$, $K_-=0$ spectrum (which overlaps with the $R(1)$, $K_-=1$ spectrum) compared to what is expected theoretically in the absence of rovibronic interactions. For other rotational transitions in this vibronic band no such deviations in the fine- and hyperfine structures are observed. Although we have not found a satisfactory explanation of the deviations from the calculated intensities in the experimental $R(0)$, $K_-=0$ spectrum in terms of rovibronic interactions, another indication that transitions to the $N'=1$ level are perturbed one way or another, is the markedly different values found for the Fermi-contact constants in the $N'=3$ and 5 rotational states (see Table I). This leads to conflicting results regarding the electronic character of the 12 658 vibronic band (see Table II). In a future publication we will discuss $K_-=1$ transitions in this, and other, vibronic bands.

For the other vibronic bands studied, no evidence is found for the presence of rovibronic interactions and we are confident that for those bands the Fermi-contact constants are a true measure of the degree of vibronic mixing of the $\tilde{X}\,^2A_1$ and $\tilde{A}\,^2B_2$ electronic states.

B. Laser induced fluorescence

Before starting the bolometer measurements we measured two vibronic bands, one at 13 510.96 cm^{-1} and the

TABLE I. Results for the $K_{-}=0$ stack of the measured vibronic bands in the energy range of 11 210–13 680 cm^{-1}. Errors are two times the standard deviation of the fit.

Band origin[a] (cm^{-1})	Int.[a] (a.u.)	Transition@freq.[b] (cm^{-1})	$\overline{\epsilon'}$ (MHz)	σ' (MHz)	λ' (MHz)
13 680.34	0.3	$R(0)$@13 681.17	-172 ± 4	94 ± 5	5 ± 6
13 510.96	0.8	$R(0)$@13 511.78 (-0.03)	2689 ± 1	96 ± 1	9 ± 1
		$R(2)$@13 513.41 (-0.04)[c]			
13 477.11	0.8	$R(0)$@13 477.90 ($+0.05$)	-240 ± 1	91 ± 1	7 ± 1
13 395.65[d]	2.5	$R(0)$@13 396.56	1086 ± 1	54 ± 1	6 ± 1
		$P(2)$@13 394.04	1086 ± 1	52 ± 1	5 ± 1
13 352.54[e]	0.25	$R(0)$@13 353.48 (-0.14)	174 ± 4	121 ± 6	9 ± 2
		$R(2)$@13 354.99 (-0.16)	217 ± 1	128 ± 7	3 ± 7
13 184.62	0.2	$R(0)$@13 185.42 ($+0.05$)	530 ± 1	89 ± 1	7 ± 1
12 724.06	0.3	$R(0)$@12 724.84	-1962 ± 1	101 ± 1	6 ± 1
		$P(2)$@12 722.17	-1963 ± 1	100 ± 1	9 ± 1
12 668.10	0.15	$R(0)$@12 668.96 (-0.05)	-107 ± 1	117 ± 1	7 ± 1
		$P(2)$@12 666.43 (-0.05)	-105 ± 2	119 ± 5	4 ± 3
12 658.34[d]	1.0	$R(0)$@12 659.28 (-0.05)	778 ± 1	43 ± 1	10 ± 1
		$P(2)$@12 656.77 (-0.07)	777 ± 1	42 ± 2	11 ± 1
		$R(2)$@12 661.15 (-0.05)	56 ± 1	61 ± 5	10 ± 4
		$P(4)$@12 655.24 (-0.05)	56 ± 1	65 ± 4	4 ± 3
		$P(6)$@12 653.91 (-0.05)	-20 ± 1	65 ± 1	7 ± 2
12 446.05	0.3	$R(0)$@12 446.90	716 ± 1	78 ± 1	5 ± 1
		$P(2)$@12 444.39	717 ± 2	79 ± 4	0 ± 6
12 340.44	0.25	$R(0)$@12 341.32	636 ± 1	100 ± 1	9 ± 1
		$R(2)$@12343.08[f]	618 ± 1	106 ± 7	3 ± 7
12 100.91[d]	0.4	$R(0)$@12 101.77	168 ± 2	99 ± 3	8 ± 2
		$P(2)$@12 099.25	166 ± 2	102 ± 3	7 ± 2
11 960.81	1.2	$R(0)$@11 961.50 ($+0.03$)	-5906 ± 1	43 ± 1	2 ± 1
		$P(2)$@11 958.98	-5908 ± 1	39 ± 1	4 ± 1
11 847.76	0.2	$R(0)$@11 848.52	1511 ± 1	116 ± 1	2 ± 1
11 807.81	0.3	$R(0)$@11 808.65	-164 ± 1	108 ± 1	9 ± 1
		$P(2)$@11 806.14	-163 ± 1	107 ± 1	10 ± 1
11 210.65[d]	0.2	$R(0)$@11 211.50[g]			
		$P(2)$@11 208.91	-1255 ± 1	81 ± 1	-8 ± 1

[a]The listed band origin and intensity are taken from the ICLAS measurements of Georges *et al.* (Ref. 4).
[b]The given frequency is the frequency corresponding to the fine structure doublet with the lowest energy. The value in parenthesis has to be added to obtain the frequency determined by Georges *et al.* (Ref. 4). It is only given when the difference is more than the accuracy of the wavemeter, i.e., 0.02 cm^{-1}.
[c]Not measured in a single scan; $\overline{B'}=0.426\ cm^{-1}$ via $R_{5/2}(2)$ [$\overline{B'}=0.426\ cm^{-1}$ (Ref. 4)]; band origin shifts toward 13 511.02 cm^{-1}.
[d]This band will be discussed in a following paper.
[e]For discussions of this vibronic band see Ref. 21.
[f]$\overline{B'}=0.434\ cm^{-1}$ (compared with $\overline{B'}=0.433\ cm^{-1}$ from Ref. 4).
[g]Only $R_{1/2}(0)$.

other at 13 395.65 cm^{-1} by laser induced fluorescence. The results from these LIF spectra are of interest since the relative fluorescence intensities give information on the composition of the vibronic bands that is complementary to that from absorption spectra and thus also from the bolometric spectra.

Of the vibronic band at 13 510.96 cm^{-1} with intensity=0.8,[4] we measured the $R(0)$ subband and, separately from each other, the two fine structure doublets of the $R(2)$ subband. For the strongest line of the $R(0)$ transition ($N''=0, J''=1/2, F''=3/2 \rightarrow N'=1, J'=3/2, F'=5/2$; see Fig. 2) we found a signal to noise ratio of 20 with a laser power of 400 mW (single pass).

For the $R(0)$ subband of this vibronic band we determined from the bolometric measurements a fine structure constant of $\overline{\epsilon'}=2689\pm1$ MHz, a Fermi-contact interaction constant of $\sigma'=96\pm1$ MHz and a dipole–dipole interaction constant of $\lambda'=9\pm1$ MHz; see Table I.

We also attempted to measure the vibronic band at 13 477.11 cm^{-1} ($\approx$742 nm), intensity=0.8,[4] but this band was not observed by LIF in our setup. We did not detect any fluorescence light in the energy window of 780 nm (cutoff filter)–900 nm (upper limit of RCA 31034 photomultiplier tube). We did measure this vibronic band, however, with the bolometer detector. The fitted constants are $\overline{\epsilon'}=-240\pm1$ MHz, $\sigma'=90\pm1$ MHz and $\lambda'=8\pm1$ MHz (Table I).

Of the vibronic band at 13 395.65 cm^{-1}, intensity=2.5,[4] we only measured the $R(0)$ transition by LIF. The strongest line in the $R(0)$ transition had a signal to noise ratio of 77 when measured with a laser power of 470 mW. The determined constants for this vibronic band are $\overline{\epsilon'}=1086\pm1$

TABLE II. Contribution of the electronic ground state in the hybrid state for the $K_{-}=0$ stack of the measured vibronic bands in the energy range of 11 210–13 680 cm^{-1}. Results are given without (''spin-unpolar.'') and with (''spin-polar.'') inclusion of spin polarization; see text for explanation. Errors are two times the standard deviation of the fit.

Band origin[a] (cm^{-1})	Int.[a] (a.u.)	Transition	Spin-unpolar. ($\tilde{X}\,^2A_1$%)	Spin-polar.[b] ($\tilde{X}\,^2A_1$%)
13 680.34	0.3	$R(0)$	64±4	66
13 510.96	0.8	$R(0)$	65±1	67
13 477.11	0.8	$R(0)$	62±1	64
13 395.65	2.5	$R(0)$	37±1	41
		$P(2)$	35±1	39
13 352.54	0.25	$R(0)$	82±4	83
		$R(2)$	87±5	88
13 184.62	0.2	$R(0)$	60±1	63
12 724.06	0.3	$R(0)$	69±1	71
		$P(2)$	68±1	70
12 668.10	0.15	$R(0)$	79±1	81
		$P(2)$	81±3	82
12 658.34	1.0	$R(0)$	29±1	34
		$P(2)$	29±1	33
		$R(2)$	41±4	45
		$P(4)$	44±3	48
		$P(6)$	44±1	48
12 446.05	0.3	$R(0)$	53±1	56
		$P(2)$	54±2	57
12 340.44	0.25	$R(0)$	68±1	70
		$R(2)$	72±5	74
12 100.91	0.4	$R(0)$	67±2	69
		$P(2)$	69±2	71
11 960.81	1.2	$R(0)$	29±1	34
		$P(2)$	26±1	31
11 847.76	0.2	$R(0)$	79±1	80
11 807.81	0.3	$R(0)$	73±1	75
		$P(2)$	73±1	74
11 210.65	0.2	$R(0)$		
		$P(2)$	55±1	58

[a]Adapted from the ICLAS measurements of Georges *et al.* (Ref. 4).
[b]Errors are the same as in the spin-restricted one-determinant approximation.

MHz, $\sigma' = 54 \pm 1$ MHz and $\lambda' = 5 \pm 1$ MHz (Table I).

The vibronic bands at 13 510.96 cm^{-1} and 13 477.11 cm^{-1} have the same intensity in absorption (ICLAS). The determined Fermi-contact interaction constants for the vibronic bands at 13 510.96 cm^{-1} and 13 477.11 cm^{-1} are $\sigma' = 96$ MHz and $\sigma' = 90$ MHz, respectively. This suggests an almost similar contribution of the electronic ground state and first electronically excited state building these excited hybrid states; see Tables I and II. On average, the fluorescence intensity, and the absorption intensity as measured by Delon *et al.*,[30] are found not to differ too much. Although the energies of both vibronic bands are close to each other, the two hybrid states must involve a (group of) different vibrational level(s) of the excited state, carrying the oscillator strength of the absorption, to explain the very different fluorescence behavior as observed in our LIF experiments. We note that we are only sensitive to the total fluorescence within the 780–900 nm window, because of the use of a cutoff filter and the sensitivity of our photomultiplier.

Comparing the signals of the $R(0)$ transitions of the vibronic bands at 13 510.96 cm^{-1} and 13 395.65 cm^{-1} (corrected for the different laser powers), the latter vibronic band is slightly more than three times as intense as the former, in good agreement with the results obtained by Georges *et al.* by ICLAS.[4]

The vibronic band at 13 395.65 cm^{-1}, although it has its major contribution from the first electronically excited state (see Table II), fluoresces too intense as to get the absorption strength from the same bright vibrational levels as the vibronic bands at 13 510.96 cm^{-1} and 13 477.11 cm^{-1}. This suggests the contribution to this hybrid state of at least one vibrational level of the first electronically excited state with a large Franck–Condon factor. In other words, this vibronic state will consist mainly of a vibrational level of the first electronically excited state with several quanta in the bending mode.[38,39] This supports the assignment of the vibronic band at 13 395.65 cm^{-1} to the $\tilde{A}\,^2B_2$ (0,5,0) state as done by Leonardi and Petrongolo.[17]

C. Character of the excited state

As stated before, the magnitude of the Fermi-contact interaction is a direct measure of the contribution of the electronic ground state to the excited vibronic state. The intensity of the vibronic band, on the other hand, is, apart from the Franck–Condon factor, determined by the contribution from the first electronically excited diabatic state. Therefore we expect a correlation between the magnitude of the Fermi-contact term and the intensity of the vibronic band. We consider this relationship in the following. The absorption spectrum, calculated by Gillispie and Khan,[38] consists of strong groups of bands, subsequent groups being separated by one quantum of the upper state bending mode (roughly 740 cm^{-1}). The strong bands are due to a relatively large Franck–Condon factor for transitions from the electronic ground state to vibrational levels in the first electronically excited state with a large number of quanta in the bending mode.

Recent theoretical calculations by Leonardi and Petrongolo[17] assign the following $\tilde{A}\,^2B_2$ excited diabatic state vibronic levels of B_2 vibronic symmetry: (0,0,0) at 9734 cm^{-1}, (0,1,0) at 10 479 cm^{-1}, (0,2,0) at 11 210 cm^{-1}, (0,3,0) at 11 960 cm^{-1}, (0,4,0) at 12 658 cm^{-1} and (0,5,0) at 13 395 cm^{-1}.

As can be seen in Fig. 4, the strong vibronic bands measured with our bolometer, assigned as the (0,5,0), (0,4,0) and (0,3,0) levels of the first electronically excited diabatic state by Leonardi and Petrongolo, have small Fermi-contact interaction constants, 54 MHz, 43 MHz and 43 MHz, respectively. This means that these relatively strong vibronic bands are dominated by the electronic character of the first electronically excited diabatic state. Because the line strength of a transition between the electronic ground state and a hybrid state is determined by the contribution of the bright electronically excited character to the hybrid state, the above mentioned vibronic bands are relatively intense due to the large Franck–Condon factors as well as to their relatively large electronically excited diabatic state character. These results are in line with the calculations by Leonardi and Petrongolo.[17]

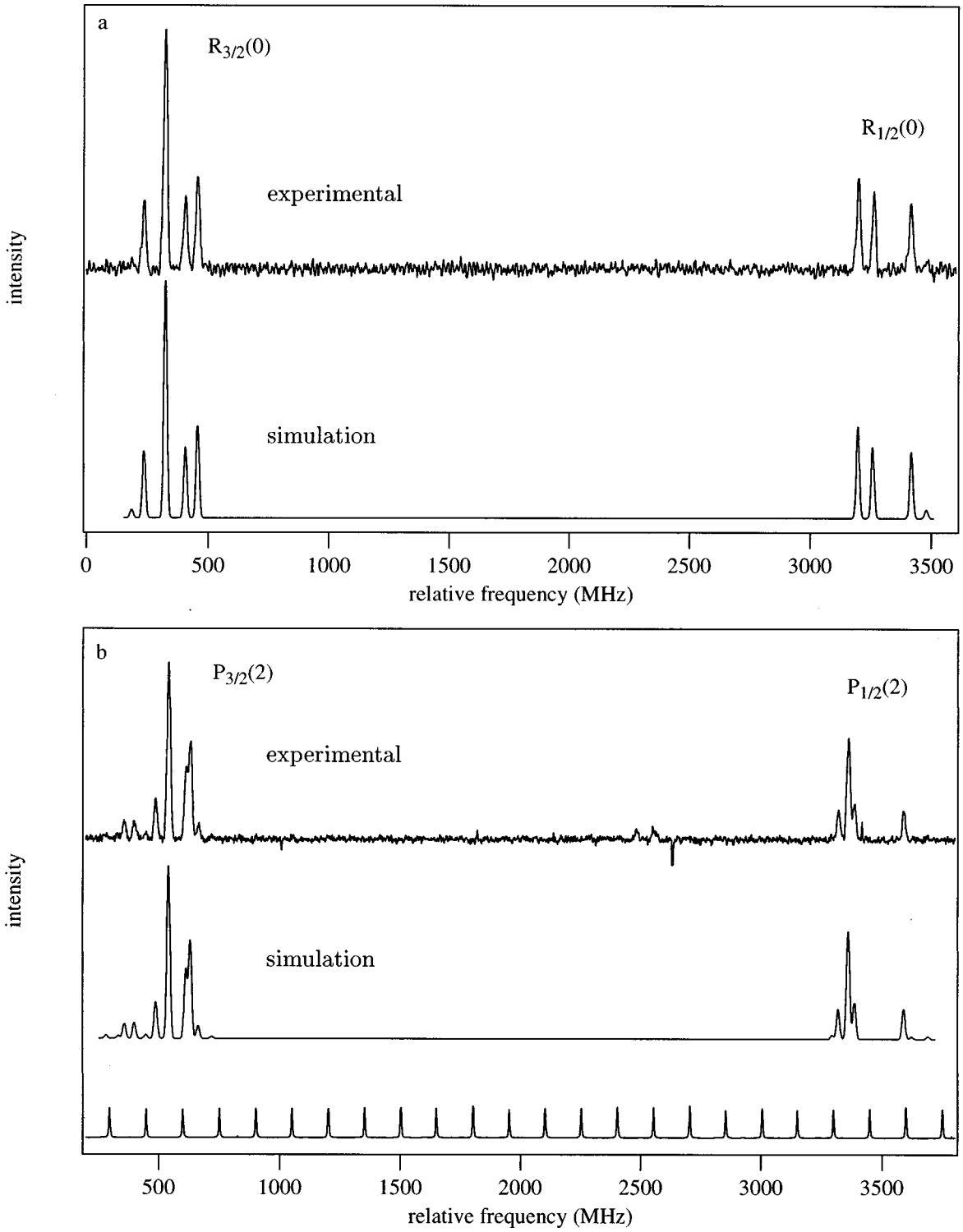

FIG. 3. Vibronic band at 12 724.06 cm^{-1}; (a) $R(0)$ subband; (b) $P(2)$ subband, the unassigned lines around 2500 MHz are transitions belonging to the $K_{-}=1$ stack.

Very recently, Jost and co-workers[6] have analyzed, and partly assigned, the observed vibronic bands in the energy region up to about 13 000 cm^{-1}, using a polyad model. The four vibonic levels at 12 100.91, 11 960.81, 11 847.76, and 11 807.81 cm^{-}, reported here (see Table I), belong to the fourth polyad, which results from two ((0,30), (1,1,0)) $\tilde{A}\,^2B_2$ zero order diabatic states. From Table II we can calculate that the sum of the percentages of $^2B_2$ character of these four observed levels amounts to 152%. This means that the remaining bright $^2B_2$ character of 48% ($2\cdot$ 100% minus 152%) in this region is dispersed over the other weaker vibronic levels in this energy region.

For the vibronic band at 11 210 cm^{-1} we find a Fermi-contact constant of 80 MHz (see Table I). This value is quite high which means that considerable ground state character has to be mixed in. This band is in the region of the third-

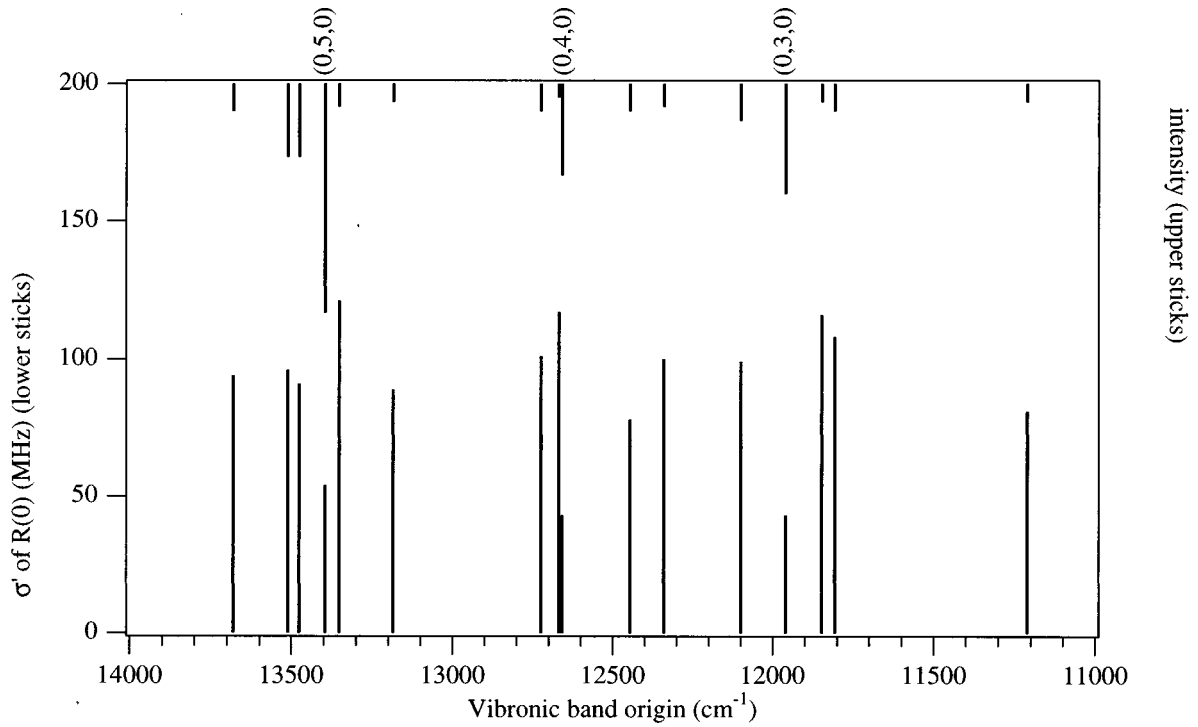

FIG. 4. Correlation between the intensities (upper sticks, measured from top axis) of the vibronic band as measured by Georges *et al.* (Ref. 4) and our measured Fermi-contact constants, σ' (lower sticks), for $N'=1$ in the excited state as a function of the energy of the vibronic band origin. A Fermi-contact constant of 147.15 MHz corresponds to 100% $\tilde{X}\,^2A_1$ electronic ground state character.

polyad[6] which results from mixing of the (0,2,0),(1,0,0) diabatic zero order $\tilde{A}\,^2B_2$ states with nearby zero order states of the $\tilde{X}\,^2A_1$ ground state.

For this vibronic band Leonardi and Petrongolo made a comparison between their calculated nonadiabatic bands[17] and the observed vibronic bands by Georges *et al.*[4] To make a comparison with our experiments, we will assume the 11 210 vibronic band to be completely described by the nearest nonadiabatic band at 11 175 cm^{-1} of the same symmetry. Leonardi and Petrongolo show that this nonadiabatic band has 49.1% $\tilde{A}\,^2B_2$ character. This contribution of the first electronically excited diabatic state almost entirely originates from the (0,2,0) vibrational level. The calculated contribution of 49.1% $\tilde{A}\,^2B_2$ in the vibronic band at 11 210 cm^{-1} is in very good agreement with 45% $\tilde{A}\,^2B_2$ contribution ($\sigma'=80$ MHz) as found in our experiments (Table II). The observed band at 11 210 cm^{-1} still has considerable ground state character. In a recent paper, Kirmse *et al.*[6] arrive at the same conclusion on the basis of the high A constant (7 ± 1 cm^{-1}) that is associated with the strong vibronic band at 11 210 cm^{-1}, which was attributed to mixing with nearby (0,13,1), (1,11,1), and (0,9,3) levels of the $\tilde{X}\,^2A_1$ ground state.

V. SUMMARY

We have analyzed the bolometric spectra of 16 vibronic bands of the $K_-=0$ stack in the energy range of 11 210–13 680 cm^{-1}. These spectra, fully resolved up to the hyperfine structure splitting, are fitted by a fine structure constant, a Fermi-contact interaction constant and a dipole–dipole interaction constant. The Fermi-contact interaction forms a very useful probe of the contribution of the electronic character of the ground state to the excited hybrid state. For the range of measured vibronic bands this contribution varies from 29% to 87%.

The effective Hamiltonian model used, includes vibronic interactions only. From the excellent agreement between the calculated intensities and the measured intensities (the intensities are not included in the fit procedure), we conclude the absence of rovibronic interactions of significant strength for the 15 measured rotational levels of the vibronic bands in the energy range of 11 210–13 680 cm^{-1}. Only for the vibronic band at 12 658 cm^{-1} are deviations observed in transitions of the $K_-=0$ stack. For this band we can fit the line positions, but we cannot explain all the intensities yet. We will address this problem in a following paper, along with other vibronic bands from the $K_-=1$ stack.

We support the assignments by Leonardi and Petrongolo[17] of the subbands at 13 395 cm^{-1}, 12 658 cm^{-1} and 11 960 cm^{-1}, respectively, to transitions to the (0,5,0), (0,4,0) and (0,3,0) vibrational levels of the first electronically excited state.

ACKNOWLEDGMENTS

We thank E. van Lenthe for calculating the Fermi-contact interaction including the spin-polarization. The Dutch Organization for Scientific Research NWO (Nederlandse Organisatie voor Wetenschappelijk Onderzoek) is thanked for its financial support through FOM. Part of the work of M.H.M.J. was made possible by a fellowship of the Royal Dutch Academy of Arts and Sciences (KNAW).

[1] G.D. Gillispie, A.U. Khan, A.C. Wahl, R.P. Hosteny, and M. Krauss, J. Chem. Phys. **63**, 3425 (1975).
[2] A. Delon and R. Jost, J. Chem. Phys. **95**, 5686 (1991).
[3] A. Delon and R. Jost, J. Chem. Phys. **95**, 5701 (1991).
[4] R. Georges, A. Delon, F. Bylicki, R. Jost, A. Campargue, A. Charvat, M. Chenevier, and F. Stoeckel, Chem. Phys. **190**, 207 (1995).
[5] A. Delon, R. Georges, B. Kirmse, and R. Jost, Faraday Discuss. **102**, 117 (1995).
[6] B. Kirmse, A. Delon, and R. Jost, J. Chem. Phys. **108**, 6638 (1998).
[7] J. Liévin, A. Delon, and R. Jost, J. Chem. Phys. **108**, 8931 (1998).
[8] H.J. Vedder, M. Schwarz, H.-J. Foth, and W. Demtröder, J. Mol. Spectrosc. **97**, 92 (1983).
[9] G. Persch, H.J. Vedder, and W. Demtröder, Chem. Phys. **105**, 471 (1986).
[10] G. Persch, H.J. Vedder, and W. Demtröder, J. Mol. Spectrosc. **123**, 356 (1987).
[11] G. Persch, E. Mehdizadeh, W. Demtröder, Th. Zimmerman, H. Köppel, and L.S. Cederbaum, Ber. Bunsenges. Phys. Chem. **92**, 312 (1988).
[12] D. Romanini, A.A. Kachanov, and F. Stoeckel, Chem. Phys. Lett. **270**, 538 (1997).
[13] G. Hirsch and R.J. Buenker, Can. J. Phys. **63**, 1542 (1985).
[14] G. Hirsch, R.J. Buenker, and C. Petrongolo, Mol. Phys. **70**, 835 (1990).
[15] G. Hirsch, R.J. Buenker, and C. Petrongolo, Mol. Phys. **73**, 1085 (1991).
[16] E. Leonardi, C. Petrongolo, V. Keshari, G. Hirsch, and R.J. Buenker, Mol. Phys. **82**, 553 (1994).
[17] E. Leonardi and C. Petrongolo, J. Chem. Phys. **106**, 10066 (1997).
[18] C.P. Blahaus, B.F. Yates, Y. Xie, and H.F. Schaefer, J. Chem. Phys. **93**, 8105 (1990).
[19] H.J. Vedder, G. Persch, and H.-J. Foth, Chem. Phys. Lett. **114**, 125 (1985).
[20] W.C. Bowman and F.C. De Lucia, J. Chem. Phys. **77**, 92 (1982).
[21] C.A. Biesheuvel, D.H.A. ter Steege, J. Bulthuis, M.H.M. Janssen, J.G. Snijders, and S. Stolte, Chem. Phys. Lett. **269**, 515 (1997).
[22] R.E. Smalley, B.L. Ramakrishna, D.H. Levy, and L. Wharton, J. Chem. Phys. **61**, 4363 (1974).
[23] H. Jalink, F. Harren, D. van den Ende, and S. Stolte, Chem. Phys. **108**, 391 (1986).
[24] W. Demtröder, *Laser Spectroscopy, Basic Concepts and Instrumentation* (Springer-Verlag, Berlin, 1982).
[25] C.S. Adams and A.I. Ferguson, Opt. Commun. **75**, 419 (1990).
[26] C.S. Adams and A.I. Ferguson, Opt. Commun. **79**, 219 (1990).
[27] B.A. Palmer, R.A. Keller, and R. Engleman, Jr., ''An Atlas of Uranium Emission Intensities in a Hollow Cathode Discharge,'' Informal report LA-8251-MS, Los Alamos Scientific Laboratories, July, 1980.
[28] I.C. Bowater, J.M. Brown, and A. Carrington, Proc. R. Soc. London, Ser. A **333**, 265 (1973).
[29] C.C. Lin, Phys. Rev. **116**, 903 (1959).
[30] A. Delon, R. Georges, and R. Jost, J. Chem. Phys. **103**, 7740 (1995).
[31] W.T. Raynes, J. Chem. Phys. **41**, 3020 (1964).
[32] R.F. Curl, Jr. and J.L. Kinsey, J. Chem. Phys. **35**, 1758 (1961).
[33] E. Haller, H. Köppel, and L.S. Cederbaum, J. Mol. Spectrosc. **111**, 377 (1985).
[34] *Numerical Recipes in Pascal*, edited by W.H. Press, B.P. Flannery, S.A. Teukolsky, and W.T. Vetterling (Cambridge University Press, Cambridge, 1989).
[35] E. van Lenthe (private communication).
[36] A. Carrington and A.D. McLachlan, *Introduction to Magnetic Resonance* (Chapman and Hall, London, 1979).
[37] E. van Lenthe, A. van der Avoird, and P.E.S. Wormer, J. Chem. Phys. **108**, 4783 (1998).
[38] G.D. Gillispie and A.U. Khan, J. Chem. Phys. **65**, 1624 (1976).
[39] K. Chen and C. Pei, Chem. Phys. Lett. **165**, 523 (1990).